Electronic ISSN: 1309-0267

International Journal of Engineering & Applied Sciences

IJEAS

Volume 12, Issue 2
2020

Published by Akdeniz University

Editorial Board

(The name listed below is not Alphabetical or any title scale)

Abstracting & Indexing

IJEAS provides unique **DOI** link to every paper published.

Editorial Scope

The journal presents its readers with broad coverage across some branches of engineering and science of the latest development and application of new solution algorithms, artificial intelligent techniques innovative numerical methods and/or solution techniques directed at the utilization of computational methods in solid and nano-scaled mechanics.

International Journal of Engineering & Applied Sciences (IJEAS) is an Open Access Journal

International Journal of Engineering & Applied Sciences (IJEAS) publish original contributions on the following topics:

Numerical Methods in Solid Mechanics

Nanomechanic and applications

Microelectromechanical systems (MEMS)

Vibration Problems in Engineering

Higher order elasticity (Strain gradient, couple stress, surface elasticity, nonlocal elasticity) Applied Mathematics

CONTENTS

International Journal of Engineering & Applied Sciences (IJEAS)
Vol. 12, Issue 2 (2020) 57-69
http://dx.doi.org/10.24107/ijeas.732172
Int J Eng Appl Sci 12(2) (2020) 57-69

Practical Jointed Approach to Functionally Graded Structures

Ibrahim KELES [a*], *Kutay AYDIN* [b]

[a] *Department of Mechanical Engineering, Samsun University, Samsun 55000, Turkey*
[b] *Department of Mechanical Engineering, Amasya University, Amasya 05100, Turkey*
**E-mail address*: ibrahim.keles@samsun.edu.tr [a], kutay.aydin@amasya.edu.tr [b]

ORCID numbers of authors:
0000-0003-3614-4877[a] *0000-0001-8252-2635* [b]

Received date: 04.05.2020
Accepted date: 10.07.2020

Abstract

In this study, a practical jointed approach in the forced vibration investigation of functionally graded material (FGM) structures under internal pressure are applied by modified Durbin's method. The FGM material consists of heterogeneous material that shows exponential variation in the thickness. Four types of dynamic loads are applied to the FGM cylinder for forced vibration. Displacement and stress distributions due to non-homogeneous constant are intended. Stress distribution dependent on the homogeneity parameter is computed and the results obtained for cylindrical structures were compared with the finite element method (FEM). The inhomogeneity parameter is empirically regulated, with a continuously changing volume fraction of the ingredients. The parameters for homogeneity were randomly selected to show displacement and stress distributions.

Keywords: Functionally graded materials, Structural elements, Boundary value problems, Modified Durbin's method

1. Introduction

The structural elements of the pressure vessels used in engineering areas such as aerospace and petroleum are important in engineering applications such as cylinder and sphere. As a result, the internal loads are one of the main problems of industrial structures. It may lead to stress gradient and / or cracked nuclei occurring in the stress distribution of the specified loads. By the analysis of the structures under the influence of the internal pressure, it facilitates the determination of the density of the points affected by the stress and the unsuitable stress distributions. Previous research has provided analytical resolutions for homogeneous isotropic and orthotropic structures. Tranter [1], Mirsky [2], Klosner and Dym [3], Ahmed [4], Ghosh [5] have pioneered their work in the cylinders, discs and spheres due to axial symmetry.

The functional graded materials (FGM) are more advanced structural materials in determining the material properties in the direction of the thickness in the solution of problems due to the composite materials interfaces. Güven [6] explained the mechanical stress distribution of the isotropic functional grade thick walled sphere under the influence of internal pressure.

Tutuncu and Ozturk [7] presented exact solutions in the form of stresses occurring in functionally graded pressure vessels. A study close to this work was also printed by Horgan and Chan [8]. Obata and Noda [9] submitted the studies of constant thermal stresses in order to understand the design of the functional graded thick-walled spheres and cylinders and the effects of the stresses. Tutuncu and Temel [10] functional-grade hollow cylinders have solved the displacements and stresses of the disc and spheres using an analytical method. Differential equations and systems obtained in the analysis of stress distributions are not easy to solve with analytical methods. In most cases, this is impossible. Therefore, numerical methods are applied in case of large equation systems, non-linearity and complex geometry. Therefore, it is a good option to select a numerical method to determine the stress distributions of FGM cylinders and spheres.

Loy et al. [11] and Pradhan et al. [12] includes the dynamic response of heterogeneous cylinders to the vibration of FGM cylindrical projectiles using the Rayleigh-Ritz method. Bayat et al. [13] presented a flexible solution for the analysis of rotating discs classified as functional in variable thickness by considering the material properties and the disc thickness profile as two power law distributions. Xiang et al. [14] presented two recursive algorithms to determine extrusion stresses between two adjacent layers in a multilayer cylinder exposed to internal and external pressure. The effects of transient waves in the FGM cylinder on stresses and displacements using the hybrid numerical method were investigated by Han et al. [15]. Assuming that FGM thick hollow cylinders are made from many bottom rollers, the finite element vibration analysis is handled by Shakeri et al. [16]. Ng et al. [17] examined the stabilization of FGM cylindrical projectiles under axial harmonic loading.

The main idea behind the modelling of FGM structural elements is to create subdivisions of material that are homogeneous in themselves with different properties as is the case with graded behavior. Although some analytical solutions (see, e.g., Keles [18])for this type of the problem is available in the literature, they either are restricted to one inhomogeneity parameter for all material properties that is not the case in real or contain complex solutions such that usually it is necessary to solve for each parameter separately, which is not practical for parametric analysis. From a parametric analysis point of view, for this type of problems numerical solution is becoming essential. In this study, we present the application of modified Durbin's method (MDM) as a numerical method for stress and displacement solutions of FGM cylinders of variable thickness. As a material feature, the change in thickness of the modulus of elasticity($E(r) = E_0 r^{\beta}$) is defined. The results were compared with FEM compared with the results. The non-homogeneous β values were used to indicate the distribution over the stress. The inhomogeneity constant β used in the study does not represent a specific material. Forced vibration analysis of structures under the influence of dynamic internal pressure changes over time through the residue theorem of Cauchy, one of the analytical solutions, is valid only for simple internal pressure loads. In this context, in order to test the accuracy of the numerical method, Keles [18] compared the solution with the literature. It is inevitable to use numerical transformation methods to determine displacement and stress distributions of structures under point, point, continuous and repulsive internal pressure. Durbin's numerical inverse Laplace transform method was chosen in this study. It is seen that this method has been applied successfully in vibration analysis for different structural elements in the literature (see for example, [19]). Laplace transformation of such loads will not be possible, especially if the internal pressure is given in point or point form. It has been found in the literature(see for example, [20, 21]) that vibration analysis is successfully applied with different methods and assumptions for the load types that are possible for Laplace transformation. In this case, Durbin's method will provide a fast and effective result. MDM is

an efficient solution procedure whose theoretical background is available in the literature [22, 23]. The method is also successfully applied in other structural mechanics problems such as those involving spherical shells [24], Timoshenko beam [25] and cylinders [26]. Dynamic behavior of cylindrical structures of different values of inhomogeneity parameter is presented. The numerical method described can be conveniently applied to FGM cylinders, discs and spherical structural members. A comparison was made with FEM (ANSYS) to determine the accuracy and effectiveness of the numerical method.

2. Basic Equation

The stress and displacement distribution in a thick-walled hollow cylinder will be considered as the inner radius *a* and the outer radius *ka* where *k* is a constant. The elasticity modules and density vary throughout the thickness as $E(r) = E_0 r^{\beta}$ and $\rho(r) = \rho_0 r^{\beta}$, respectively. The subscripted terms in Table 1 that is ()i and ()o are the material properties of FGM thick-walled hollow cylinder.

Table 1. Material properties of the FGM thick-walled hollow cylinder.

E_0 (GPa)		206		ρ_0 (g/cm^3)		7.85	
	β	r(m)	$()_i$ =1	$()_o$ =2	β	r(m)	$()_i$ =1	$()_o$ =2
	-5		206	6.437	-5		7.85	0.2453
$E(r)=E_0 r^{\beta}$	-2		206	51.5	$\rho(r)= \rho_0 r^{\beta}$ -2		7.85	1.9625
(GPa)	0		206	206	(g/cm^3) 0		7.85	7.85
	2		206	824	2		7.85	31.4
	5		206	6592	5		7.85	251.2

2.1. Basic Formulation of FGM Cylinders

Strain-displacement and basic equations considering the assumption of plane strain are [7]

$$\varepsilon_r = \frac{du}{dr}, \qquad \varepsilon_\theta = \frac{u}{r}, \tag{1}$$

$$\sigma_r = C_{11}(r)\varepsilon_r + C_{12}(r)\varepsilon_\theta,$$
$$\sigma_\theta = C_{12}(r)\varepsilon_r + C_{11}(r)\varepsilon_\theta, \tag{2}$$

where, with ν_0 the Poisson's ratio,

$$C_{11}(r) = \left(\frac{E_0(1-\nu_0)}{(1+\nu_0)(1-2\nu_0)}\right) r^{\beta}$$

and

$$C_{12}(r) = \left(\frac{E_0\nu_0}{(1+\nu_0)(1-2\nu_0)}\right) r^{\beta}.$$

The only nontrivial equilibrium equation under assumptions can be inscribed in the following form [5],

$$\frac{\partial \sigma_r}{\partial r} + \frac{\sigma_r - \sigma_\theta}{r} = \rho_0 r^{\beta} \frac{\partial^2 u}{\partial t^2} \tag{3}$$

Using Eqs. (1) - (3), basic equation of radial displacement becomes

$$\frac{r^2\partial^2 u}{\partial r^2} + r\frac{\partial u}{\partial r}m_1 + m_2 u = \frac{r^2}{c^2}\frac{\partial^2 u}{\partial t^2} \tag{4}$$

where $c^2 = \frac{\left(\frac{E_0(1-v_0)}{(1+v_0)(1-2v_0)}\right)}{\rho_0}$,$m_1 = \beta + 1$,$m_2 = \frac{v_0\beta}{(1-v_0)} - 1$

with boundary conditions in radial directions

$$\sigma_r|_{r=a} = -P \text{ and } \sigma_r|_{r=ka} = 0 \tag{5}$$

Converting the dimensionless variables

$$v = \frac{u}{a}, x = \frac{r}{a}, \tau = \frac{ct}{a} \tag{6}$$

reduces Eq. (4) in the form

$$\frac{\partial^2 v}{\partial x^2} + \frac{m_1}{x}\frac{dv}{dx} + \frac{m_2}{x^2}v = \frac{\partial^2 v}{\partial \tau^2} \tag{7}$$

and boundary conditions are as follows

$$\sigma_r|_{x=1} = -P(\tau) \quad \sigma_r|_{x=k} = 0 \tag{8}$$

with the primary conditions

$$v = 0 \text{ and } \frac{\partial v}{\partial \tau} = 0 \text{ when } \tau = 0 \qquad \text{for} \quad 1 \le x \le k \tag{9}$$

The general equation of displacement in Laplace space takes the following form:

$$\bar{v}(x,p) = \text{£}\,[v(x,\tau)] = \int_0^\infty v(x,\tau)e^{-p\tau}\,d\tau \tag{10}$$

where *p* is the Laplace parameter. Eq. (7) is converted to Laplace space by applying initial conditions to obtain the following equation:

$$\frac{d^2\bar{v}}{dx^2} + \frac{m_1}{x}\frac{d\bar{v}}{dx} + \left(\frac{m_2}{x^2} - p^2\right)\bar{v} = 0 \tag{11}$$

The final form of boundary conditions in Laplace space will take the form

$$\bar{\sigma}_r|_{x=1} = -\bar{P}(p)\bar{\sigma}_r|_{x=k} = 0 \tag{12}$$

Solution of Eq. (11) Bessel function expression

$$\bar{v}(x,p) = x^{\phi}(C_1 I_n(px) + C_2 K_n(px)) \tag{13}$$

where I_n and K_n are Bessel functions of first and second kind, respectively, of order *n* with

$\phi = -\frac{\beta}{2}, n = \sqrt{1 - \frac{v_0\beta}{1-v_0} + \frac{\beta^2}{4}},$

The final solution of the final solution using the iteration formulas (e.g. see reference [27]) in Laplace space by obtaining C_1 and C_2 by applying the general equation obtained without dimension using boundary conditions is as follows;

$$\bar{v}(x,p) = -\frac{\bar{P}(p)}{C_{11}} x^{\phi} \frac{F(p)}{G(p)} \tag{14}$$

where

$$F(p) = [K_n(pk)S_1 + pkK_{n-1}(pk)]I_n(px) - [I_n(pk)S_1 - pkI_{n-1}(pk)]K_n(px) \tag{15}$$

and

$$\begin{aligned} G(p) = [K_n(pk)S_1 + pkK_{n-1}(pk)][I_n(p)S_1 - pI_{n-1}(p)] \\ -[K_n(p)S_1 + pK_{n-1}(p)][I_n(pk)S_1 - pkI_{n-1}(pk)] \end{aligned} \tag{16}$$

where $S_1 = (n - m - \phi)$ and $m = \frac{C_{12}(r)}{C_{11(r)}}$

For displacement distribution in the FGM cylinder subject to internal pressure, Eq. 14 in Laplace space must be converted to real time space.

3. Numerical Inversion of Solution by the Modified Durbin's Method (MDM)

The numerical solution of forced vibration analysis for the FGM cylinder was obtained for a set value of the Laplace parameter. For the conversion of results to time space, the modified Durbin method is used. The inverse Laplace transformation method that provides the conversion of Durbin to time space is expressed as [18, 28]:

The meaning $f(t)$ at time t_j is assumed by

$$f(t_j) \cong \frac{2Exp[aj\Delta t]}{T} \begin{bmatrix} -\frac{1}{2} Re\{\bar{F}(a)\} \\ + Re\left\{\sum_{k=0}^{N-1} (\bar{F}(p_k)L_k) Exp[i(\frac{2\pi}{N})jk]\right\} \end{bmatrix}, (j=0,1,2,\dots N\text{-}1) \tag{17}$$

where $\bar{F}(p_k)$ is the Laplace transform of $f(t)$. The k*th* Laplace parameter is demarcated as $p_k = a + ik\frac{2\pi}{T}$. The number N is$N = \frac{T}{\Delta t}$ where T is the solution recess and Δt is the time raise. The choice of constant 'a' is done by transmission a value to aT. It is proposed that the value of aT be in the range 5 to 10. For the mathematical samples offered in this paper this value is taken as 6. Finally, the results are adapted by multiplying each term in the precis by Lanczos factor L_k as recommended in (e.g. see reference [29]).

$$L_k = \frac{Sin(\frac{k\pi}{N})}{(\frac{k\pi}{N})}, (L_0=1) \tag{18}$$

If the Laplace transform of the function $f(t)$ is not given in closed-form as in the case of point-by-point definition, the discrete values need first to be transformed into the Laplace domain as follows:

$$\bar{F}(p_k) = \Delta t \sum_{n=0}^{N-1} [f(t_n) e^{-at_n}] \, e^{-i\frac{2\pi nk}{N}} \tag{19}$$

For various pressures only the term $\bar{P}(p)$ is altered in the solution certain by Eq. (14).

4. Implementation Disc and Spherical Structures

The expressions given the preceding sections can readily be used for solutions of FGM annular disks in plane stress with the material constants in Eq. (2) redefined as

$$C_{11}(r) = \frac{E_0}{1+{v_0}^2} r^{\beta}, \qquad C_{12}(r) = \frac{E_0 v_0}{1+{v_0}^2} r^{\beta} \tag{20}$$

As for FGM spheres structure; u is

$$\varepsilon_r = \frac{\partial u}{\partial r} \text{ and } \varepsilon_\theta = \varepsilon_\varphi = \frac{u}{r} \tag{21}$$

Expressions between stress-strain are

$$\begin{gathered} \sigma_r = C_{11}\varepsilon_r + C_{12}\varepsilon_\theta + C_{12}\varepsilon_\varphi = C_{11}(r)\varepsilon_r + 2C_{12}(r)\varepsilon_\theta \\ \sigma_\theta = \sigma_\varphi = C_{12}\varepsilon_r + C_{11}\varepsilon_\theta + C_{12}\varepsilon_\varphi = C_{12}(r)\varepsilon_r + (C_{12}(r) + C_{11}(r))\varepsilon_\theta \end{gathered} \tag{22}$$

The radial displacement solution given for the FGM cylinder is still legal with the next constraints now redefined as

$$\phi = -(\tfrac{1+\beta}{2}), n = \sqrt{\phi^2 - 2(\tfrac{v_0\beta}{1-v_0} - 1)}, \; m = \tfrac{C_{12}(r)}{C_{11}(r)}, \; S_1 = (n - 2m - \phi) \tag{23}$$

5. Results

Figures (1,6) show comparison of the methods and evolution of circumferential stress σ_θ and radial displacement v for $\nu = 0.3, k = 2.0$ and $\beta = -5.0, -2.0, 0.0, 2.0, 5.0$ The boundary conditions for stresses are assumed as $\bar{\sigma}_r|_{x=1} = -\bar{P}(p), \bar{\sigma}_r|_{x=k} = 0$. In accordance with the material and geometric properties used in the numerical method model, commercial (ANSYS) finite element code was compared and generated [29]. Due to the symmetry in the cylinder, four of the four geometries formed in the finite element model are considered. In the finite element model, an 8-axis axial symmetric rectangular element is used. For the modeling of the cylindrical structures FGM, each layer was applied with 20 layers having a fixed material property value.

Results obtained by Keles [18] are used for validation purposes, analytical. The comparing will be illustrated in the Tables 2-3. It can be observed form Tables, the results are in good agreement with the same results from Keles [18] It is proven that upon a screening results

given in Tables 2-3, a substantial amount of accuracy and efficiency is achieved using the MDM method.

Table 2. Comparison of MDM results with Keles [18] for the radial displacements with different dynamic loads applied to the inner surface of the cylinder. (β = 0.0, ω = 1.0 ,γ=1.0, k=2.0)

τ	$P_1(\tau) = P_0(1 - Cos(\omega\tau))$ $v\ C_{11} / P_0$		$P_2(\tau) = P_0$ $v\ C_{11} / P_0$		$P_3(\tau) = P_0(1 - e^{-\gamma\tau})$ $v\ C_{11} / P_0$	
	Keles [18]	MDM	Keles [18]	MDM	Keles [18]	MDM
0	0	0,000003	0	0,00001	0	0,000001
5	6,54644	6,54643	4,88701	4,88700	4,17045	4,17043
10	-2,11269	-2,11267	0,07458	0,07456	0,83551	0,83550
15	5,33630	5,33629	4,78081	4,78079	4,26004	4,26002
20	-0,66194	-0,66191	0,23675	0,23674	0,76713	0,76710
25	7,32722	7,32720	4,62315	4,62313	4,30325	4,30323
30	-0,91986	-0,91984	0,42225	0,42224	0,73963	0,73960
35	5,09853	5,09851	4,49282	4,49280	4,3124	4,31239
40	-1,80397	-1,80396	0,55301	0,55300	0,73936	0,73934
45	6,66612	6,66610	4,44839	4,44837	4,30764	4,30762
50	0,16580	0,16579	0,58978	0,58976	0,74312	0,74310

Table 3. Comparison of MDM results with Keles [18] for the hoop stresses with different dynamic loads applied to the inner surface of the cylinder. (β = 0.0, ω = 1.0 ,γ=1.0, k=2.0)

τ	$P_1(\tau) = P_0(1 - Cos(\omega\tau))$ σ_θ / P_0		$P_2(\tau) = P_0$ σ_θ / P_0		$P_3(\tau) = P_0(1 - e^{-\gamma\tau})$ σ_θ / P_0	
	Keles [18]	MDM	Keles [18]	MDM	Keles [18]	MDM
0	0	0,000003	-0,41145	-0,41142	0,00002	0,00001
5	5,09078	5,09076	3,60494	3,60491	3,01761	3,01760
10	-2,51242	-2,51241	-0,35857	-0,35855	0,26815	0,26812
15	3,655910	3,655909	3,51747	3,51743	3,08857	3,08855
20	-0,79378	-0,79373	-0,22501	-0,22500	0,21180	0,21179
25	6,03100	6,03099	3,38763	3,38761	3,12415	3,12413
30	-1,11281	-1,11280	-0,07223	-0,07220	0,18916	0,18914
35	3,39960	3,39959	3,28029	3,28028	3,13169	3,13166
40	-2,18586	-2,18582	0,03545	0,03543	0,18894	0,18893
45	5,29085	5,29083	3,24369	3,24367	3,12777	3,12776
50	0,12184	0,12182	0,06574	0,06572	0,19204	0,19202

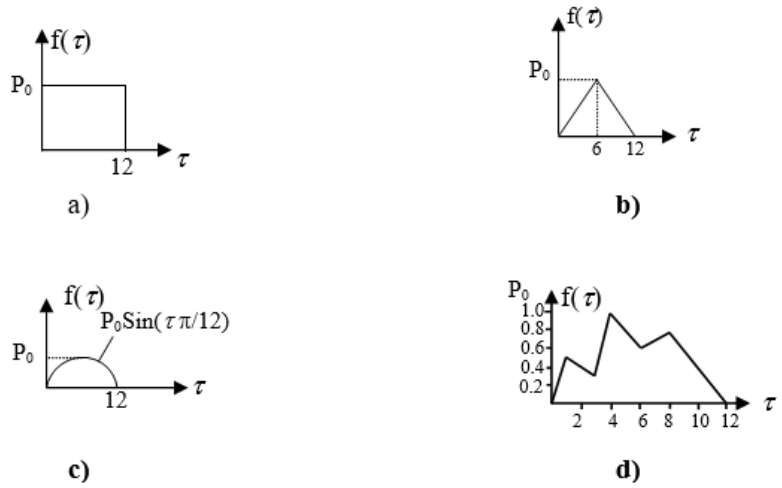

Fig. 1. Dynamic loads: (**a**) rectangular impulsive load, (**b**) triangular impulsive load, (**c**) half sinus impulsive load (**d**) impulsive load given discretely

In this study, results are offered for many impulsive deployed loads. Four cases of impulsive loadings (rectangular impulsive load, triangular impulsive load, half sinus impulsive load, impulsive load given discretely step) are considered (see Fig. 1). Figs. 2 and 3 show the effect of rectangular impulsive load on the radial displacements and circumferential stress of the suggested method and FEM. In Figs. 2 and 3, displacement decreases with increasing inhomogeneity parameter. Second, the triangular impulsive load is considered. Figs. 4 and 5 include displacements in the problem solved by the numerical method used and ANSYS software. As β increases, a decrease occurs in the value of circumferential stress in Figs. 4-5. When the numerical results of radial displacements and tangential stresses are compared with the results obtained with MDM and FEM, it is seen that the results are almost identical. Third, the half sinus impulsive load is considered. A collation of damping of radial displacement and stress are obtainable in Figs. 6-7. If the inhomogeneity constant is positive, it expresses the increase of hardness by providing stress protective effect in the radial direction. Finally, the impulsive load given discretely is considered. The radial displacements and circumferential stress of FG cylinder for inhomogeneity constant ($\beta = -5.0, -2.0, 0.0, 2.0, 5.0$) are presented in Figs. 8-9. It is clearly obvious that the radial displacements and circumferential stress for all approaches are identical (Figs. 8–9). It is seen that the results of Durbin's method solutions are overlapping with the model created using a commercial finite element code, FEM [30].

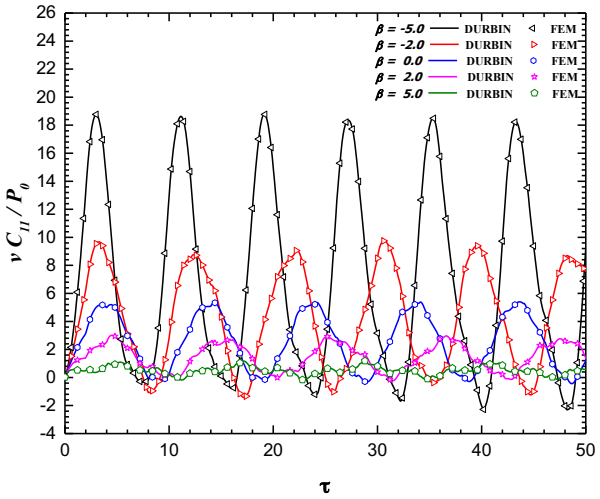

Fig. 2. Radial displacement versus time for rectangular impulsive load

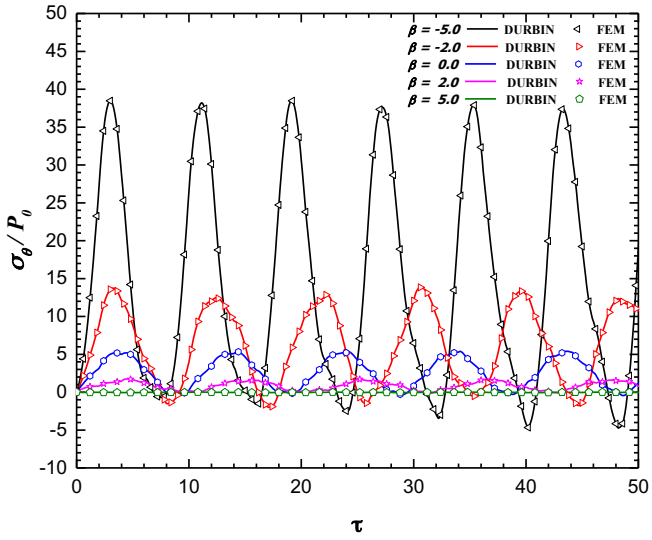

Fig. 3. Hoop stress versus time for rectangular impulsive load

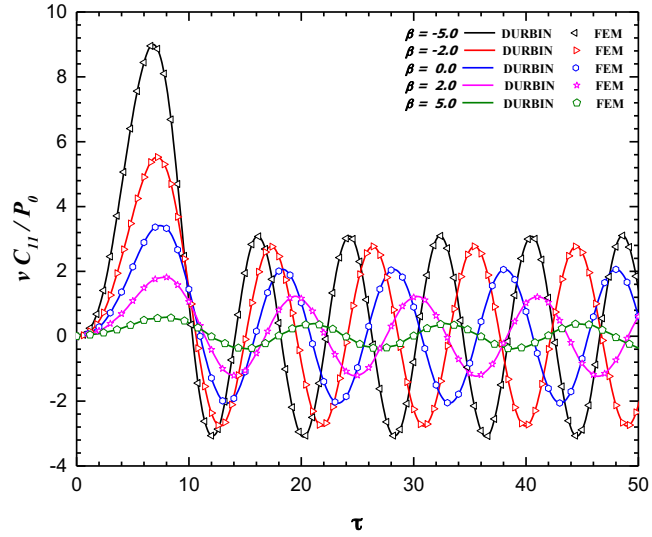

Fig. 4. Radial displacement versus time for triangular impulsive load

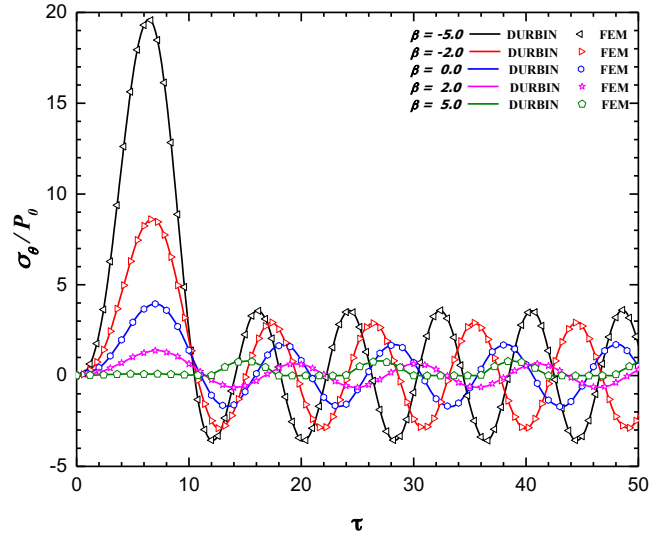

Fig. 5. Hoop stress versus time for triangular impulsive load

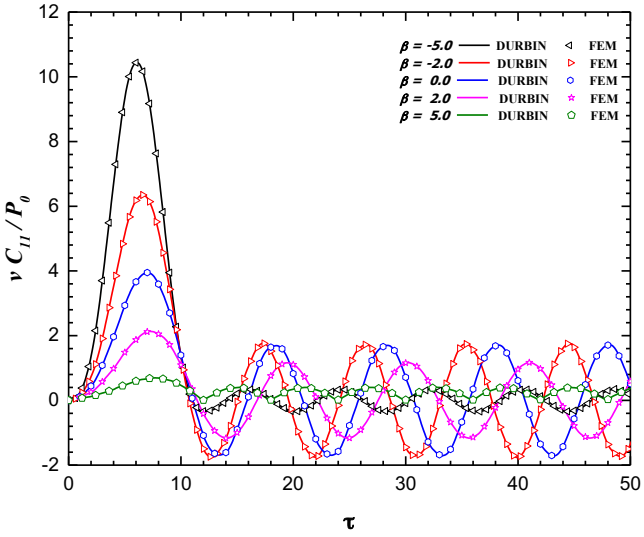

Fig. 6. Radial displacement versus time for half sinus impulsive load

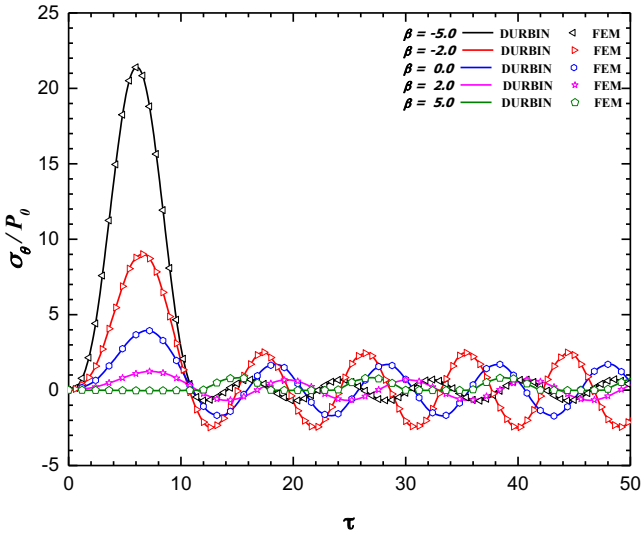

Fig. 7. Hoop stress versus time for half sinus impulsive load

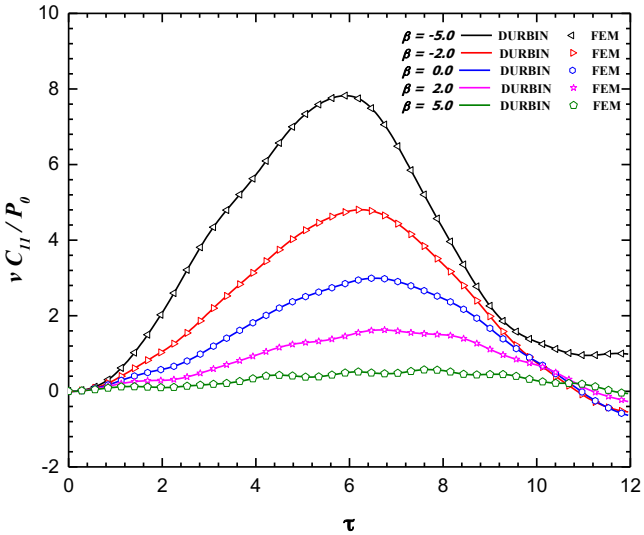

Fig. 8. Radial displacement versus time for impulsive load given discretely

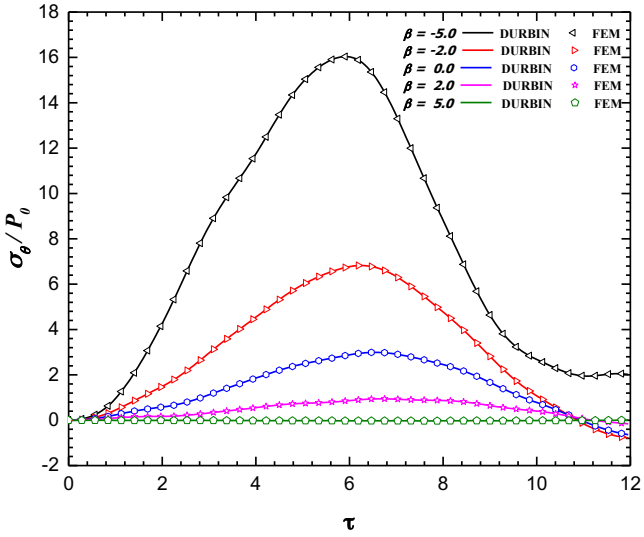

Fig. 9. Hoop stress versus time for impulsive load given discretely

6. Conclusion

Numerical model of FGM cylinders for stresses and displacement are obtained and solved by Durbin's method. The efficacy and adequacy of the present method is first compared to analytical results presented for constant Elastic Modulus and Poisson Ratio. The solution procedure can be applied to any continuous grading function option. The solution technique and procedure are simple, efficient and well structured, in addition to providing low cost accuracy. We have seen that FGM thick-walled cylindrical engineering structures with exponential variable properties have a significant effect on mechanical behavior. In particular, the positive inhomogeneity constant has a major effect on the stress distribution. Although the inhomogeneity parameter is a useful parameter in design, it can be applied for special applications in order to control stress distributions and displacement

References

[1] Tranter, C., LXV. The application of the Laplace transformation to a problem on elastic vibrations. *The London, Edinburgh, and Dublin Philosophical Magazine and Journal of Science,* 33, 614-622, 1942

[2] Mirsky, I., Axisymmetric vibrations of orthotropic cylinders. *The Journal of the Acoustical Society of America,* 36, 2106-2112, 1964

[3] Klosner, J.M. and C.L. Dym, Axisymmetric, Plane- Strain Dynamic Response of a Thick Orthotropic Shell. *The Journal of the Acoustical Society of America,* 39, 1-7, 1966

[4] Ahmed, N., Axisymmetric Plane- Strain Vibrations of a Thick- Layered Orthotropic Cylindrical Shell. *The Journal of the Acoustical Society of America,* 40, 1509-1516, 1966

[5] Ghosh, A., Axisymmetric vibration of a long cylinder. *Journal of sound and vibration,* 186, 711-721, 1995

[6] Güven, U.u., On stress distributions in functionally graded isotropic spheres subjected to internal pressure. *Mechanics Research Communications,* 3, 277-281, 2001

[7] Tutuncu, N. and M. Ozturk, Exact solutions for stresses in functionally graded pressure vessels. *Composites Part B: Engineering,* 32, 683-686, 2001

[8] Horgan, C. and A. Chan, The pressurized hollow cylinder or disk problem for functionally graded isotropic linearly elastic materials. *Journal of Elasticity,* 55, 43-59, 1999

[9] Obata, Y. and N. Noda, Steady thermal stresses in a hollow circular cylinder and a hollow sphere of a functionally gradient material. *Journal of Thermal stresses,* 17, 471-487, 1994

[10] Tutuncu, N. and B. Temel, A novel approach to stress analysis of pressurized FGM cylinders, disks and spheres. *Composite Structures,* 91, 385-390, 2009

[11] Loy, C., K. Lam, and J. Reddy, Vibration of functionally graded cylindrical shells. *International Journal of Mechanical Sciences,* 41, 309-324, 1999

[12] Pradhan, S., C. Loy, K. Lam, and J. Reddy, Vibration characteristics of functionally graded cylindrical shells under various boundary conditions. *Applied Acoustics,* 61, 111-129, 2000

[13] Bayat, M., M. Saleem, B. Sahari, A. Hamouda, and E. Mahdi, Analysis of functionally graded rotating disks with variable thickness. *Mechanics Research Communications,* 35, 283-309, 2008

[14] Xiang, H., Z. Shi, and T. Zhang, Elastic analyses of heterogeneous hollow cylinders. *Mechanics Research Communications,* 33, 681-691, 2006

[15] Han, X., G. Liu, Z. Xi, and K. Lam, Transient waves in a functionally graded cylinder. *International Journal of Solids and Structures,* 38, 3021-3037, 2001

[16] Shakeri, M., M. Akhlaghi, and S. Hoseini, Vibration and radial wave propagation velocity in functionally graded thick hollow cylinder. *Composite structures,* 76, 174-181, 2006

[17] Ng, T., K. Lam, K. Liew, and J. Reddy, Dynamic stability analysis of functionally graded cylindrical shells under periodic axial loading. *International Journal of Solids and Structures,* 38, 1295-1309, 2001

[18] Keles, I., *Elastic response of FGM and anisotropic thick-walled pressure vessels under dynamic internal pressure*. 2007, PhD thesis, Cukurova University.

[19] Çalım, F.F., Dynamic analysis of beams on viscoelastic foundation. *European Journal of Mechanics-A/Solids,* 28, 469-476, 2009

[20] Celebi, K., I. Keles, and N. Tutuncu, Closed-Form Solutions For Forced Vibration Analysis of Inhomogenous Rod. 2012

[21] Celebi, K., I. Keles, and N. Tutuncu, Exact Solutions for Forced Vibration of Non-Uniform Rods by Laplace Transformation. *Gazi University Journal of Science,* 24, 347-353, 2011

[22] Temel, B. and M.F. Şahan, Transient analysis of orthotropic, viscoelastic thick plates in the Laplace domain. *European Journal of Mechanics-A/Solids,* 37, 96-105, 2013

[23] Liang, X., Y. Deng, Z. Cao, X. Jiang, T. Wang, Y. Ruan, and X. Zha, Three-dimensional dynamics of functionally graded piezoelectric cylindrical panels by a semi-analytical approach. *Composite Structures,* 226, 111176, 2019

[24] Şahan, M.F., Viscoelastic damped response of cross-ply laminated shallow spherical shells subjected to various impulsive loads. *Mechanics of Time-Dependent Materials,* 21, 499-518, 2017

[25] Wu, J.-S. and L.-K. Chiang, Out-of-plane responses of a circular curved Timoshenko beam due to a moving load. *International Journal of Solids and Structures,* 40, 7425-7448,

2003

[26] Daneshjou, K., M. Bakhtiari, and A. Tarkashvand, Wave propagation and transient response of a fluid-filled FGM cylinder with rigid core using the inverse Laplace transform. *European Journal of Mechanics-A/Solids,* 61, 420-432, 2017

[27] Watson, G.N., *A treatise on the theory of Bessel functions*. 1995: Cambridge university press.

[28] Durbin, F., Numerical inversion of Laplace transforms: an efficient improvement to Dubner and Abate's method. *The Computer Journal,* 17, 371-376, 1974

[29] Narayanan, G.V., *Numerical Operational Methods in Structural Dynamics*. 1981, PhD thesis, University of Minnesota.

[30] ANSYS Swanson Analysis System, Inc., 201 Johnson Road, Houston, PA 15342-1300, USA.,

International Journal of Engineering & Applied Sciences (IJEAS)
Vol. 12, Issue 2 (2020) 70-77
http://dx.doi.org/10.24107/ijeas.772707
Int J Eng Appl Sci 12(2) (2020) 70-77

Effect of Slenderness Ratio on Fatigue Life of CFRP Strengthened Steel I-Beam

Md. Shariful Islam [a], Md. Abdul Hasib[b]*

[a,b]Department of Mechanical Engineering, Khulna University of Engineering & Technology, Khulna, Bangladesh.
[*]E-mail address: sharifulmekuet@gmail.com [a], ahasib@me.kuet.ac.bd [b*]

ORCID numbers of authors:
0000-0003-2851-871X[a], 0000-0002-2915-7840[b]

Received date: 21.07.2020
Accepted date: 30.09.2020

Abstract

Carbon fiber reinforced polymers (CFRP) to repair and strengthen the steel I-beam has been increasingly used since last decade. CFRP composites bonded to steel members offer many advantages over steel plate bonding including excellent corrosion resistance, high stiffness and high strength to weight ratios etc. This study numerically investigates the fatigue performance of CFRP strengthened steel I-beam. One non-strengthened control beam and several strengthened beams using steel plates and CFRP strips were investigated primarily. The effect of slenderness ratios of web on fatigue behavior of CFRP strengthened steel I-beam is investigated. The beams were simulated in full three-dimension and fatigue life was investigated by using general-purpose finite element program, ANSYS. Simply supported beam subjected to two loads on compression flange is analyzed to show the effect of CFRP and slenderness ratios on fatigue behavior of steel I beam. The results show, that the life cycle of a CFRP strengthened beam before failure is higher than that of bare beam. It is also observed that beams with higher slenderness ratios (fixed thickness of the web) give better fatigue performance.

Keywords: CFRP, I-beam, Fatigue, Slenderness ratio.

1. Introduction

Strengthening of steel structural member with carbon fiber reinforced polymer (CFRP) has gained much research attraction last couple of years. The structures used in bridges of railway and highway, marine industry may experience deterioration over time due to lots of reasons like environmental effects, corrosion, fatigue, high intensity loading, and gradual loss of strength with time, etc. The deterioration due to fatigue of structural member has become a major challenge faced by different infrastructure, bridge and other industries. FRP externally bonded to structures possesses many advantages such as high strength to weight ratio, high corrosion resistance or resistance to oxidation, high durability, ease of installation etc. Among different FRP, carbon fiber and glass fiber have shown more stability in strengthening structural members.

Numerous experiments have been carried out on the behavior of steel or concrete beams reinforced with CFRP plates. Conventionally steel plates are added to the bottom flange of I-beam. In similar fashion CFRP laminates are also added to the tension flange for flexural

strengthening. Edberg et al. carried out experimental investigations on some different configurations of strengthened beam, with CFRP and GFRP. The results obtained in both cases were observed, and it found that CFRP laminated beams show more strength than GFRP laminated beams. In other words, CFRP strengthening is more effective than GFRP strengthening [1]. Tavakkolizadeh et al. also investigated the fatigue performance of CFRP strengthened steel girders [2]. They showed that CFRP strengthened beam has much higher life than with strengthening, in fact, they found three times life in CFRP strengthened beam. Also, crack growth rates are decreased significantly. Dawood et al investigated the primary behavior of scaled bridge beams of steel-concrete combination strengthened with HM CFRP materials [3]. They compared their results with analytical models based on the fundamental principles of equilibrium and compatibility. Fernando et al conducted several studies on the fatigue strengthening of steel beams using fiber reinforced polymer and they showed the overall performance of beam strengthened with CFRP [4]. They also investigated the fatigue behavior of cracked steel beams with externally bonded CFRP laminates. Kim et al investigated fatigue behavior of intentionally created notched beam strengthened with CFRP in Finite element method and predicted the fatigue life based on strain life theory [5]. Finally, they propose an empirical model to predict fatigue behavior of the interface. Xie et al investigated the fatigue behavior of CFRP strengthened beam equipped with three-point bending [6]. An empirical formula was developed to predict the fatigue life of CFRP strengthened beam based on experimental observation. Colombi et al performed fatigues tests on cracked steel plates strengthened on one side and evaluated fatigue crack propagation curves by integrating paris law and finally compared this with experimental data [7]. Wang et al investigated experimentally the fatigue behavior of bonded surface between steel plates and carbon fiber reinforced polymer laminate [8]. It is observed that fatigue life is very much responsive to adhesive thickness and fatigue life increases with increase in adhesive thickness. El-Emam et al used ultra-high modulus (UHM) CFRP laminates to enhance the fatigue life of pre-cracked steel beams [9]. They found positive results in UHM carbon fiber reinforced polymer and the life is much increased with UHM CFRP. Effects of significant parameters like the slenderness ratio of web of I-beam on fatigue performance are yet to be analyzed.
In this paper fatigue performance of CFRP strengthened steel I-beams is observed. The effect of the slenderness ratio of web of CFRP strengthened I-beam is investigated.

2. Materials and Methods

2.1. Materials

In this analysis, steel I-beam of grade ASTM(A36) is strengthened by CFRP strip and steel plate as well to investigate the fatigue performance of CFRP. Table 1 shows material properties of the I-beams. Fig. 1 indicates the dimensions of the steel I-section. The steel plates used for flexural reinforcement and stiffener are of the same grade as the steel I-beams. Steel plate A is installed on the bottom flange by using adhesive (Sikadur-30). The dimensions of the steel plates, CFRP and adhesive are shown in table 2. CFRP materials have high tensile strength which can improve the structural behavior of structures. Normally, CFRP

Table 1: Mechanical properties of structural steel [10].

Young's Modulus (MPa)	Poisson's Ratio	Strength	
		Yield Strength (MPa)	Tangent Modulus (MPa)
210000	0.3	250	1450

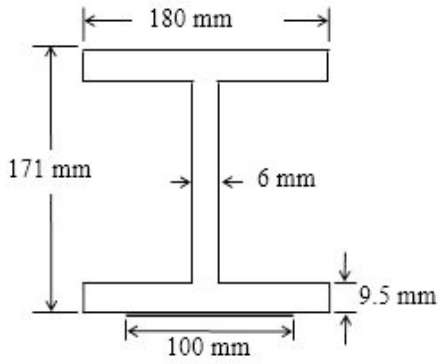

Fig.1. Dimensions of steel I-Section.

Table 2: Dimensions of steel plate, CFRP and adhesive.

	Width (mm)	Length (mm)	Thickness (mm)
Plate A	100	1500	6,8
CFRP	100	1500	1.2
Adhesive	100	1500	1

Table 3: Properties of CFRP [11,12].

Parameter	Value
Young's modulus in *X* direction (MPa)	310000
Young's modulus in *Y* direction (MPa)	11200
Young's modulus in *Z* direction (MPa)	11200
Poisson's Ratio *XY*	0.0058
Poisson's Ratio *YZ*	0.3
Poisson's Ratio *XZ*	0.0058
Shear Modulus *XY* (MPa)	26500
Shear Modulus *YZ* (MPa)	3700
Shear Modulus *XZ* (MPa)	26500
Tensile strength (MPa)	3100

is produced in the form of a strip (plate) or a sheet (wrap). In this study, CFRP strip is installed on the tensile region to improve the fatigue performance of structures. Table 3 shows material properties of the CFRP, which is orthotropic in behavior

2.2. Finite Element Model

This analysis is performed by the general-purpose finite element program, Ansys v18.1. All the parts, including I section, CFRP, steel plate and adhesive, in the Finite element analysis, were modelled using higher order 3D 20 nodes solid elements, SOLID186. The beam is supported with simply supported condition as shown in fig 3. There are two supports at two ends, one is pin support another is roller support. In pin support displacements in the x, y and z direction is restricted but moments in these directions are not restricted i.e. free to rotate. On the other hand, in roller support displacement in y direction is restricted but there are five

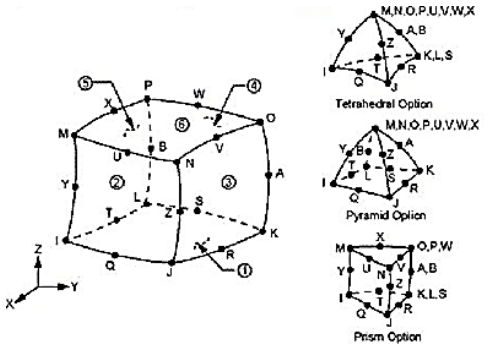

Fig. 2. Solid 186 element type in Ansys [13].

degrees of freedom this support. Two loads of equal magnitude are applied at the top of the compression flange along lines. The beam's free span is 1.8 m and the length of the CFRP sheets adhered to the tension flange is 1.5 m. The free length between the end of the CFRP and the supports is not strengthened. For fatigue life estimation S-N curve is used and S-N curve for steel and CFRP are shown in fig. 4.

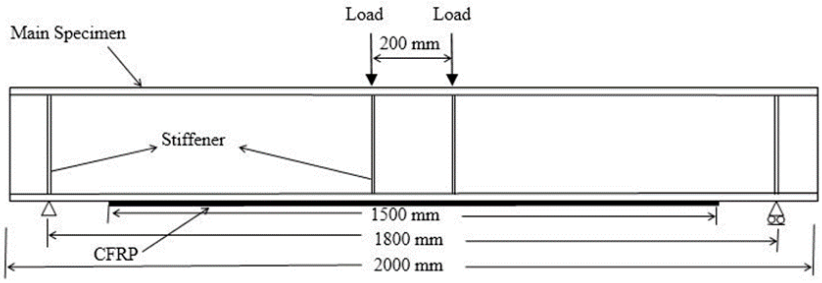

Fig. 3. Specifications of the strengthened steel I-beam.

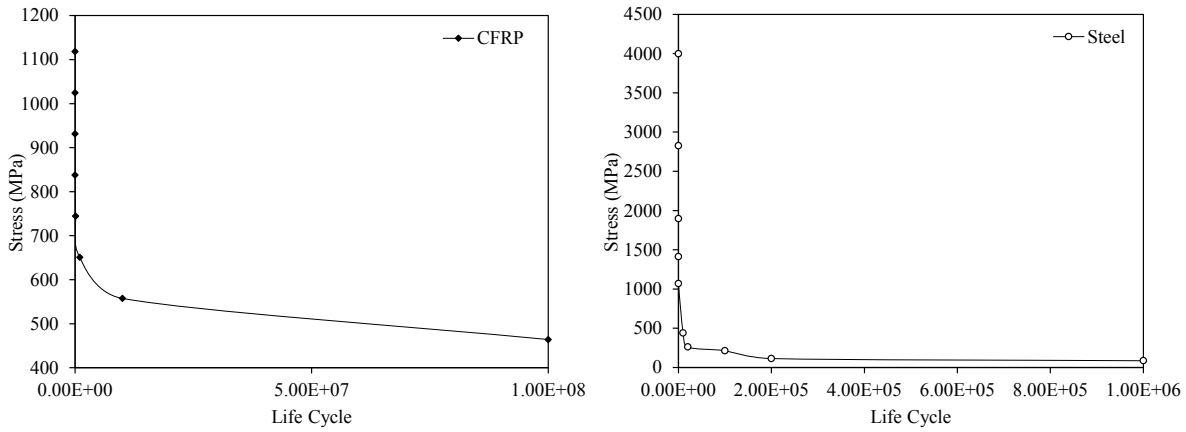

(a) (b)

Fig. 4. S-N curve for (a) CFRP [13] and (b) Steel [14]

2.3. Model Validation

The model is investigated by using a general-purpose finite element program, ANSYS. To validate the present model, the specimen was equipped and material properties were taken as of reference specimen from literature. The load-deflection curve at midspan of the without strengthening beam is compared with the experimental result as shows in fig. 5(a). It is observed that the present study maintains a very good agreement with the reference beam from literature.

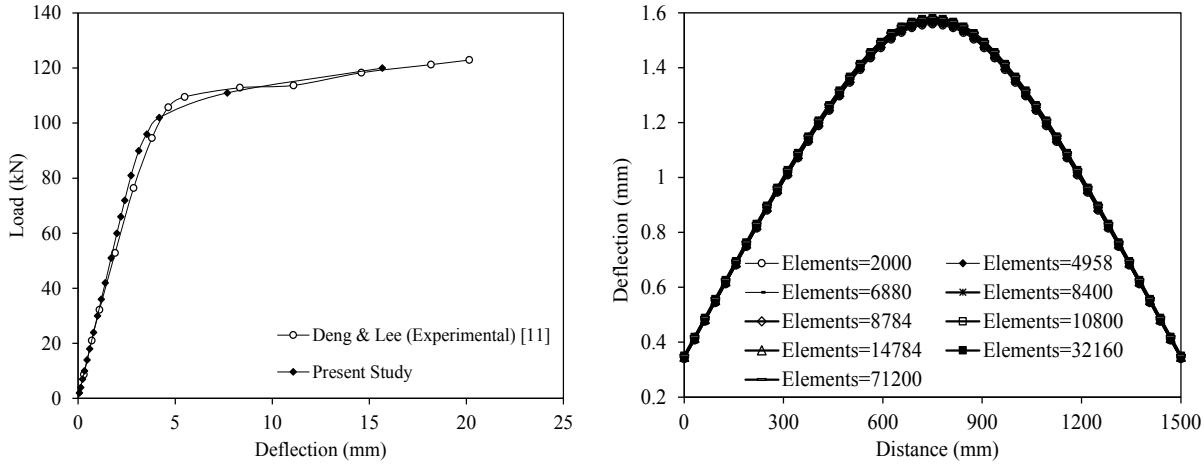

Fig. 5. (a) Load-deflection curves for previous study and present study, (b) Deflection along the length of CFRP for different element counts.

2.4. Mesh Independence Test

To obtain independent mesh for the further analysis a result is compared to different meshing combination. In this case deflections along the length of the beam for a specific loading condition for different elements are shown in fig. 5(b). It is found that for different elements and nodes the change in deflection is very little or negligible. That indicates independence of the model. Finally, a model with elements of 32160 was selected for further analysis.

3. Results and Discussions

3.1. Effect of CFRP on Fatigue Life

In order to show the effect of CFRP on life expectancy the fatigue life for bare beam, steel plate strengthened beams and CFRP strengthened beam are compared as shown in fig. 6. It is obvious from figure that the minimum life, at which any part of the beam will fail before design life is reached for CFRP strengthened beam is much higher than that of the bare beam and steel plate strengthened beams.

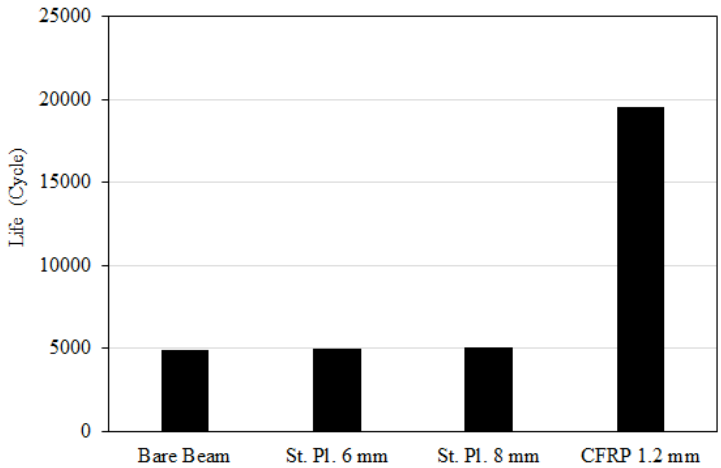

Fig. 6. Estimated life for the load of 100 kN for bare beam and strengthened beams.

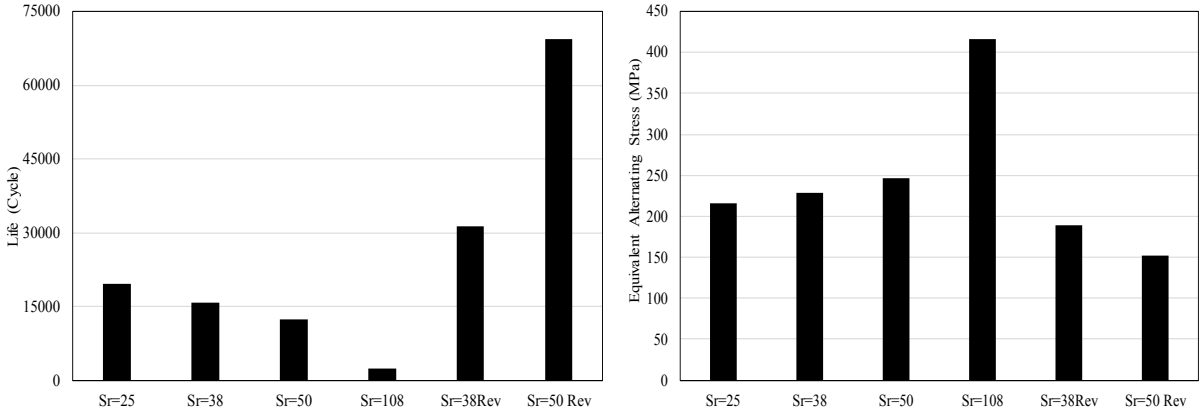

(a) (b)

Fig. 7. (a) Estimated life, and (b) Equivalent alternating stress for the load of 100 kN for different Slenderness ratios

3.2. Fatigue life and Equivalent Alternating Stress

Fig. 7(a) depicts the fatigue life for different slenderness ratio ranging from 25 to 108. With the increase in slenderness ratios with a fixed height of the web, life cycle of the beam before failure decreases. But, when slenderness ratio is increased with a fixed width of the web, then life cycle of the beam increases. Fig. 7(b) shows the equivalent alternating stresses for different slenderness ratios. It is observed that with the increase in the slenderness ratio from 25 to 108 with varying width of the web, the equivalent alternating stress increases, but when slenderness ratio is increased with varying height of the beam, equivalent alternating stress decreases.

3.3. Fatigue Sensitivity

Fatigue sensitivity analysis shows, how fatigue life will respond with change of load at a certain range. In this analysis, fatigue sensitivity analysis is done in the range of 50% of load to 150% of load. Fatigue sensitivity analysis is performed for different slenderness ratios. With the increase in the slenderness ratio keeping the height of the web fixed, the life cycle is

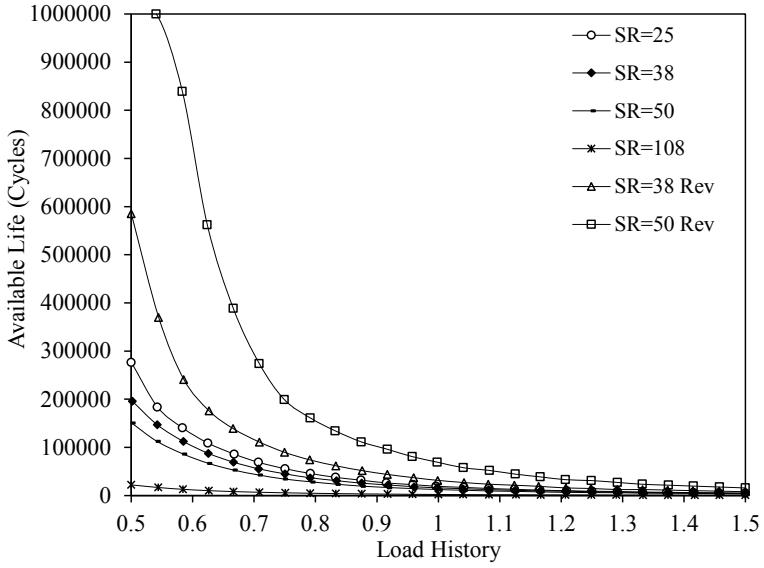

Fig. 8. Comparison of fatigue sensitivity for 100 kN load among slenderness ratios.

decreased for all loading condition. At the same time, while the slenderness ratio is increased keeping fixed the width of the web, life cycle is increased. Fig. 8 depicts available life cycle for different slenderness ratios, where 1 indicates the original loading(100kN) and 1.5 indicates 150kN and so on.

4. Conclusions

In this study fatigue performance of steel I-beam strengthened with carbon fiber reinforced polymer (CFRP) is analyzed numerically. CFRP laminates and steel plates are added to the bottom of the steel I beam to strengthen the member. One bare beam along with strengthened beams using CFRP laminates and steel plates are investigated. Specific outcomes of this investigation are-

- o Life cycle that a beam can sustain under fatigue loading, before failure for CFRP strengthened is higher than that of bare beam.
- o Beams with higher slenderness ratios (fixed thickness of the web) give better fatigue performance.

References

[1] Edberg, W., Mertz, D., Gillespie, J., Rehabilitation of steel beams using composite materials. *ASCE fourth materials engineering conference,* Washington D.C., United States, 1996.

[2] Tavakkolizadeh, M., Saadatmanesh, H.S., Fatigue strength of steel girders reinforced with carbon Fibre reinforced polymer patch. *Journal of Structural Engineering*, 129, 186–196. 2003.

[3] Dawood, M., Rizkalla, S., Sumner, E., Fatigue and Overloading Behavior of Steel–Concrete Composite Flexural Members Strengthened with High Modulus CFRP Materials. *Journal of Composites for Construction,* 11, 659-669, 2007.

[4] Fernando, D., Schumacher, A., Motavalli, M. fatigue strengthening of cracked steel beams with cfrp plates. *Proceedings of the ASME 2010 International Mechanical Engineering Congress & Exposition*, Vancouver, British Columbia, Canada, 2010.

[5] Kim, Y.J., Harries, K.A., Fatigue behavior of damaged steel beams repaired with CFRP strips. *Engineering Structures*, 33, 1491–1502, 2011.

[6] Xie, J.h., Xin, P.Y.H., Guo, X.Y., Fatigue behavior of reinforced concrete beams strengthened with prestressed fibre reinforced polymer. *Construction and Building Materials*, 27, 149–157, 2012.

[7] Colombia, P., Favaa, G., Poggia, C., Fatigue reinforcement of steel elements by CFRP materials: experimental evidence, analytical model and numerical simulation. *Procedia Engineering*, 74, 384–387, 2014.

[8] Wang, H.T., Wu, G., Pang, Y.Y., Experimental study on the bond behavior between CFRP plates and steel substrates under fatigue loading. *Composites Part B: Engineering,* 176, 1-12, 2019.

[9]. El-Emam, H., Mustafic, M., Salim,H., Elsisi, A., Sallam, H., Fatigue Life Enhancement for Steel Girders Using Ultra-High Modulus Carbon Fiber-Reinforced Polymer, *ASCE Structures Congress*, Reston, United States, 2019.

[10] ASTM A36 Steel Properties, Modulus of Elasticity, Yield Strength, Material Density, Hardness & Equivalent, *US ASTM AISI and Save Standards*, World Material.

[11] Deng, J., Jun Deng, Lee, M.M.K, Moy, S.S.j., Stress analysis of steel beams reinforced with a bonded CFRP plate. *Composite Structures*, 65, 205-215, 2004.

[12] SIKA® Product Information, S.e., Sika® Kimia Sdn Bhd., Kuala Lumpur.

[13] Zaharia, S.M., Morariu, C.O., Nedelcu, A., Pop, M.A., Experimental Study of Static and Fatigue Behavior of CFRP-Balsa Sandwiches under Three-point Flexural Loading*, Bio Resources,* 12, 2673-2689, 2017.

[14] Library, Ansys Workbench Module.

International Journal of Engineering & Applied Sciences (IJEAS)
Vol. 12, Issue 2 (2020) 78-87
http://dx.doi.org/10.24107/ijeas.782419
Int J Eng Appl Sci 12(2) (2020) 78-87

A Solution Method for Longitudinal Vibrations of Functionally Graded Nanorods

Büşra Uzun [a], M. Özgür Yaylı [b]*

[a,b] Bursa Uludag University, Engineering Faculty, Department of Civil Engineering Division of Mechanics, Bursa-TURKEY

[*]E-mail address: buzun@uludag.edu.tr [a*], ozguryayli@uludag.edu.tr [b]

ORCID numbers of authors:
0000-0002-7636-7170[a], 0000-0003-2231-170X[b]

Received date: 19.08.2020
Accepted date: 06.10.2020

Abstract

In the present study, a nonlocal finite element formulation of free longitudinal vibration is derived for functionally graded nano-sized rods. Size dependency is considered via Eringen's nonlocal elasticity theory. Material properties, Young's modulus and mass density, of the nano-sized rod change in the thickness direction according to the power-law. For the examined FG nanorod finite element, the axial displacement is specified with a linear function. The stiffness and mass matrices of functionally graded nano-sized rod are found by means of interpolation functions. Functionally graded nanorod is considered with clamped-free boundary condition and its longitudinal vibration analysis is performed.

Keywords: Nonlocal elasticity theory, Functionally graded materials, Nanorod, Finite element method, Vibration

1. Introduction

One of the popular structures of recent times is functionally graded (FG) composite materials. The difference of these materials which are usually a combination of metal and ceramic from traditional laminated composites is that the smooth changing of material properties. In functionally graded materials, the material properties like Young's modulus, density, shear modulus etc. change according to a certain rule continuously along at least one direction. Thanks to this smooth property changing, functionally graded materials have been precious for many applications such as biomedical, chemistry, electronics, optics, aircraft, space vehicles and biology etc. [1,2]. In addition, functionally graded structures have attracted considerable attention in models of nano/micro mechanics. The studies on functionally graded nano/micro structures such as FG nanoplate [3-7], FG nanobeam [8-14], FG nanorod [14-18] have been presented by researchers in recent years.

In addition to the analytical solution [19,20], many other methods like discrete singular convolution method [21,22], polynomial differential quadrature method [23], finite difference method, finite element method [24] etc. have been used by researchers to solve a problem. In this study, a finite element formulation for free longitudinal vibration behavior of functionally graded nanorod is presented. Small-scale effect of the functionally graded nanorod is discussed based on the nonlocal elasticity theory. The nonlocal elasticity theory has an additional small-scale parameter (nonlocal parameter) and thanks to this nonlocal parameter the small-scale effects occurring in nano/micro-sized structures can be evaluated. The nonlocal elasticity theory has become a frequently performed theory in nanomechanics and micromechanics, as it allows the consideration of small-scale effects. In addition, articles using finite element method to examine the behavior of size-dependent microstructures/nanostructures such as vibration [25-30], buckling [29-32] and bending [29-30, 33-35] are also found in the literature.

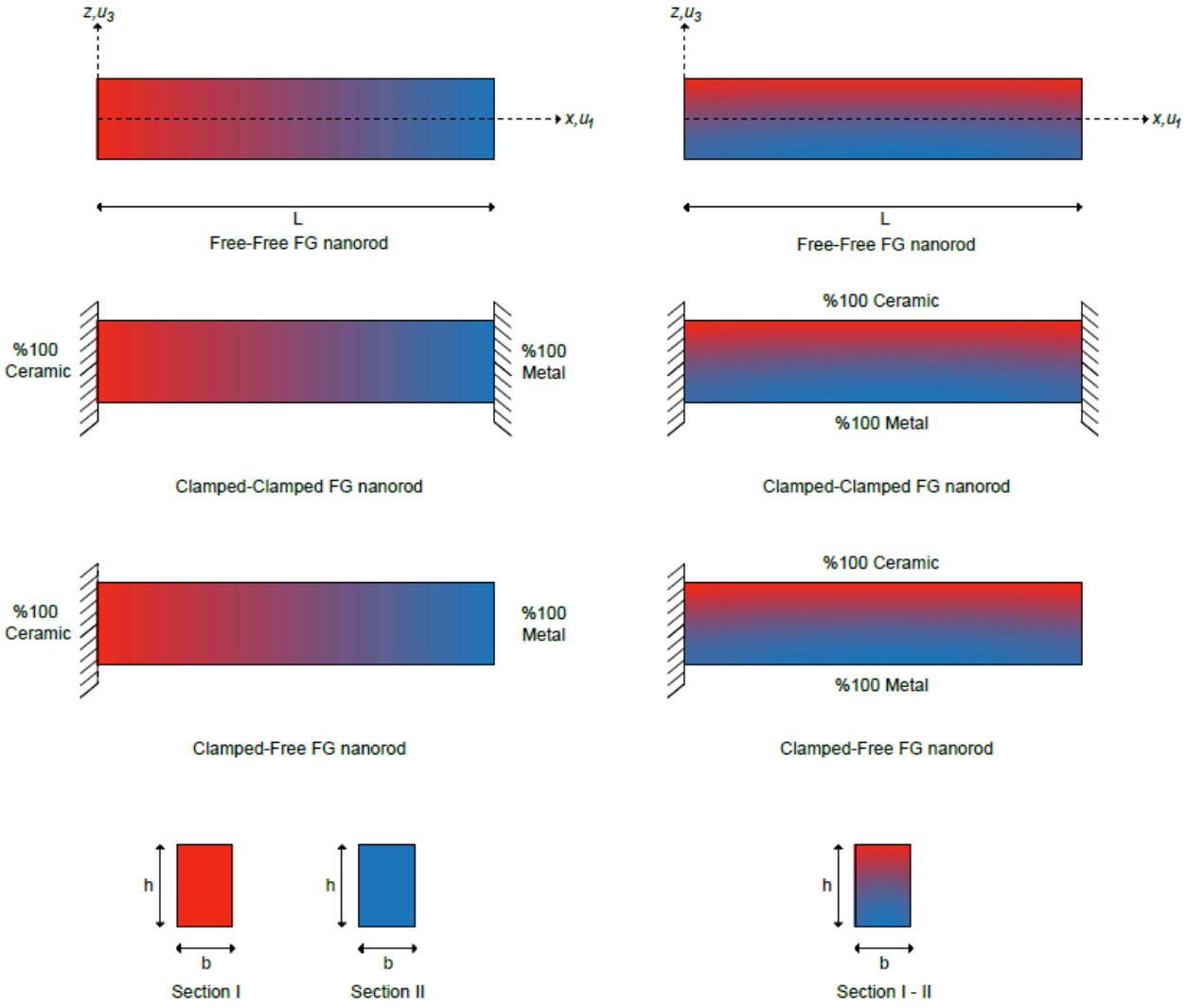

a) Type - I b) Type - II

Fig. 1. Functionally graded nanorods with various boundary conditions

2. Functionally Graded Rod

FG nanorods with various boundary conditions like free-free, clamped-clamped and clamped-free are illustrated in Figure 1. *L*, *b* and *h* represent the length, width and thickness of the FG rod, respectively. Type I (Fig. 1a) and Type II (Fig. 1b) represent the FG nanorods whose material properties vary continuously in the axial direction and thickness direction, respectively. The material properties such as Young's modulus, density etc. change of the rod according to a power-law. If the changing of material properties of the rod is assumed in the thickness direction, the effective material properties of rod can be defined as [11, 13]

$$P(z) = (P_c - P_m)\left(\frac{z}{h} + \frac{1}{2}\right)^k + P_m \tag{1}$$

Where, *P* represents the effective material property, while *k* represents the non-negative power-law exponent. The subscripts *c* and *m* indicate the ceramic and metal materials, respectively. u_1, u_2 and u_3 are the displacements of the FG rod in the *x*, *y*, *z* directions, respectively, and may be written as follow

$$u_1(x,z,t) = u(x,t), \quad u_2(x,z,t) = 0, \quad u_3(x,z,t) = 0 \tag{2}$$

u, and *t* denote the axial displacement of any point on the neutral axis and time, respectively. Stress (σ) and normal force (*N*) expressions for the FG rod are written as follows

$$\sigma_{xx} = E(z)\varepsilon_{xx} \tag{3}$$

$$N = \int_A \sigma_{xx}(z)\,dA \tag{4}$$

Here, ε and *A* are strain and cross-section area, respectively. The equations of motions of FG nano-sized rod can be obtained by means of the Hamilton's principle [36]

$$\int_{t_1}^{t_2} (\delta K - \delta U + \delta W)\,dt = 0 \tag{5}$$

Where *U, K* and *W* are the strain energy, kinetic energy and work done by external forces, respectively. The external loads can be encountered as elastic foundation, axial compressive force, thermal loading etc. However, there are no external forces in this vibration problem of FG nanorod and so *W* is set to zero. The first variations of the strain energy and kinetic energy are given as follows

$$\delta\int_{t_1}^{t_2} U dt = \int_{t_1}^{t_2}\int_0^L N\delta\left(\frac{\partial u}{\partial x}\right)dxdt \tag{6}$$

$$\delta\int_{t_1}^{t_2} K dt = \int_{t_1}^{t_2}\int_0^L I_0 \frac{\partial u}{\partial t}\delta\left(\frac{\partial u}{\partial t}\right)dxdt \tag{7}$$

Here, I_0 is expressed as

$$I_0 = \int_A \rho(z)dA, \tag{8}$$

By substituting equations (6) - (7) into equation (5) and after some mathematical arrangements, we obtain the equation of motion of the rod as follows

$$\delta u : \frac{\partial N}{\partial x} = I_0 \frac{\partial^2 u}{\partial t^2} \tag{9}$$

3. Size-Dependent Finite Element Formulation

The nonlocal constitutive formulation is [37]

$$\left[1-\left(e_0 a\right)^2 \nabla^2\right]\sigma_{ij} = C_{ijkl}\varepsilon_{kl} \tag{10}$$

Where σ_{ij} is the stress tensor, C_{ijkl} is the fourth-order Young's modulus tensor, ε_{kl} is the strain tensor, $e_0 a$ is the nonlocal parameter. The Equation (10) can be rewritten as

$$\sigma_{xx} - \left(e_0 a\right)^2 \frac{\partial^2 \sigma_{xx}}{\partial x^2} = E(z)\varepsilon_{xx} \tag{11}$$

Integrating Eq. (11) over the cross-section area, we obtain the axial force-strain relation as Eq. (12)

$$N - (e_0 a)^2 \frac{\partial^2 N}{\partial x^2} = A_1 \frac{\partial u}{\partial x} \tag{12}$$

Here, A_1 is expressed as

$$A_1 = \int_A E(z)dA, \tag{13}$$

Differentiating Equation (9) with respect to x, then substituting into Equation (12) we obtain Equation (14).

$$N = A_1 \frac{\partial u}{\partial x} + (e_0 a)^2 I_0 \frac{\partial^3 u}{\partial x \partial t^2} \tag{14}$$

By substituting Equation (14) into Equation (9), the equation of the motion of FG nanorod is obtained as

$$A_1 \frac{\partial^2 u}{\partial x^2} + (e_0 a)^2 I_0 \frac{\partial^4 u}{\partial x^2 \partial t^2} - I_0 \frac{\partial^2 u}{\partial t^2} = 0 \tag{15}$$

In this study, a rod finite element is considered has two nodes. ϕ is the interpolation (or shape) functions matrix of a rod finite element and expressed as below

$$[\phi] = \left[1 - \frac{x}{L} \quad \frac{x}{L}\right] \tag{16}$$

The stiffness matrix, classical mass and nonlocal mass matrices are obtained using Eqs. (15) - (16) as follows

$$K = \int_0^L A_1 \left([\phi]'\right)^T [\phi]' \, dx \tag{17}$$

$$M_{cl} = \int_0^L I_0 \left([\phi]\right)^T [\phi] dx \tag{18}$$

$$M_{nl} = (e_0 a)^2 \int_0^L I_0 \left([\phi]'\right)^T [\phi]' \, dx \tag{19}$$

In the above Equations, superscript *T* represents the transpose operator. The subscripts *cl* and *nl* are used to indicate the classical and nonlocal theories, respectively. The frequencies of FG nano-sized rod are found as follows

$$\left|K - \omega_n^2 \left(M_{nl} + M_{cl}\right)\right| = 0 \tag{20}$$

Here ω_n and the subscript *n* indicate the circular frequency and mode number.

4. Numerical Results

In this section, comparison studies and numerical examples are performed. Comparison studies are presented by Xu et al. [38] and Numanoğlu et al. [39]. Table 1 is presented to compare the validity of the method and to show the compatibility with each other. Comparisons of non-dimensional frequencies for the first four modes of clamped-free homogeneous nanorods are shown in Table 1. Also, this Table demonstrates the effect of the number of finite element (*N*) on convergence. As can be seen, the number of finite elements is an important issue for the convergence of frequency values. The appropriate number of elements should be chosen to ensure desired convergence. As can be seen, low number of finite elements provides the desired convergence for low modes. However, it may be

necessary to increase the number of finite elements as the mode number increase. Dimensionless parameters used in the comparison studies are defined as follows

$$\bar{\omega}_n = \omega_n L\sqrt{\rho / E}, \quad \bar{\mu} = e_0 a / L \tag{21}$$

Table 1. Comparison of dimensionless frequencies of homogeneous nanorod

$\bar{\mu}$	$\bar{\omega}_n$	Xu et al. [38]	Numanoğlu et al. [39]	Present study (N=200)	Present study (N=100)	Present study (N=50)	Present study (N=20)
0.0	*n=1*	1.57080	1.57080	1.5708	1.5708	1.5709	1.5712
	n=2	4.71239	4.71239	4.7125	4.7128	4.7141	4.7233
	n=3	7.85398	7.85398	7.8545	7.8560	7.8621	7.9045
	n=4	10.99557	10.99557	10.9970	11.0011	11.0177	11.1345
0.1	*n=1*	1.55177	1.55177	1.5518	1.5518	1.5518	1.5522
	n=2	4.26279	4.26279	4.2629	4.2631	4.2641	4.2709
	n=3	6.17668	6.17668	6.1769	6.1777	6.1806	6.2012
	n=4	7.39805	7.39805	7.3985	7.3997	7.4048	7.4399
0.2	*n=1*	1.49858	1.49858	1.4986	1.4986	1.4986	1.4989
	n=2	3.42933	3.42933	3.4294	3.4295	3.4300	3.4335
	n=3	4.21782	4.21782	4.2179	4.2181	4.2191	4.2256
	n=4	4.55152	4.55152	4.5516	4.5519	4.5531	4.5612

In this section, effects of power-law exponent and the nonlocal parameter on the free vibration response of functionally graded nanorod are investigated. In the numerical calculations, the number of finite elements for FG nanorod is chosen as 200. Functionally graded nanorod is considered composed of aluminum and alumina and with clamped-free boundary condition. The top and bottom surfaces of the nanorod are composed of pure alumina (ceramic) and aluminum (metal), respectively. Mechanical properties of functionally graded nanorod constituents are given as [40]: E_m=70 GPa, ρ_m=2700 kg/m^3 for aluminum and E_c=393 Gpa, ρ_c=3960 kg/m^3 for alumina. The following dimensionless frequency parameter is used

$$\lambda_n = \omega_n L\sqrt{\rho_c / E_c} \tag{22}$$

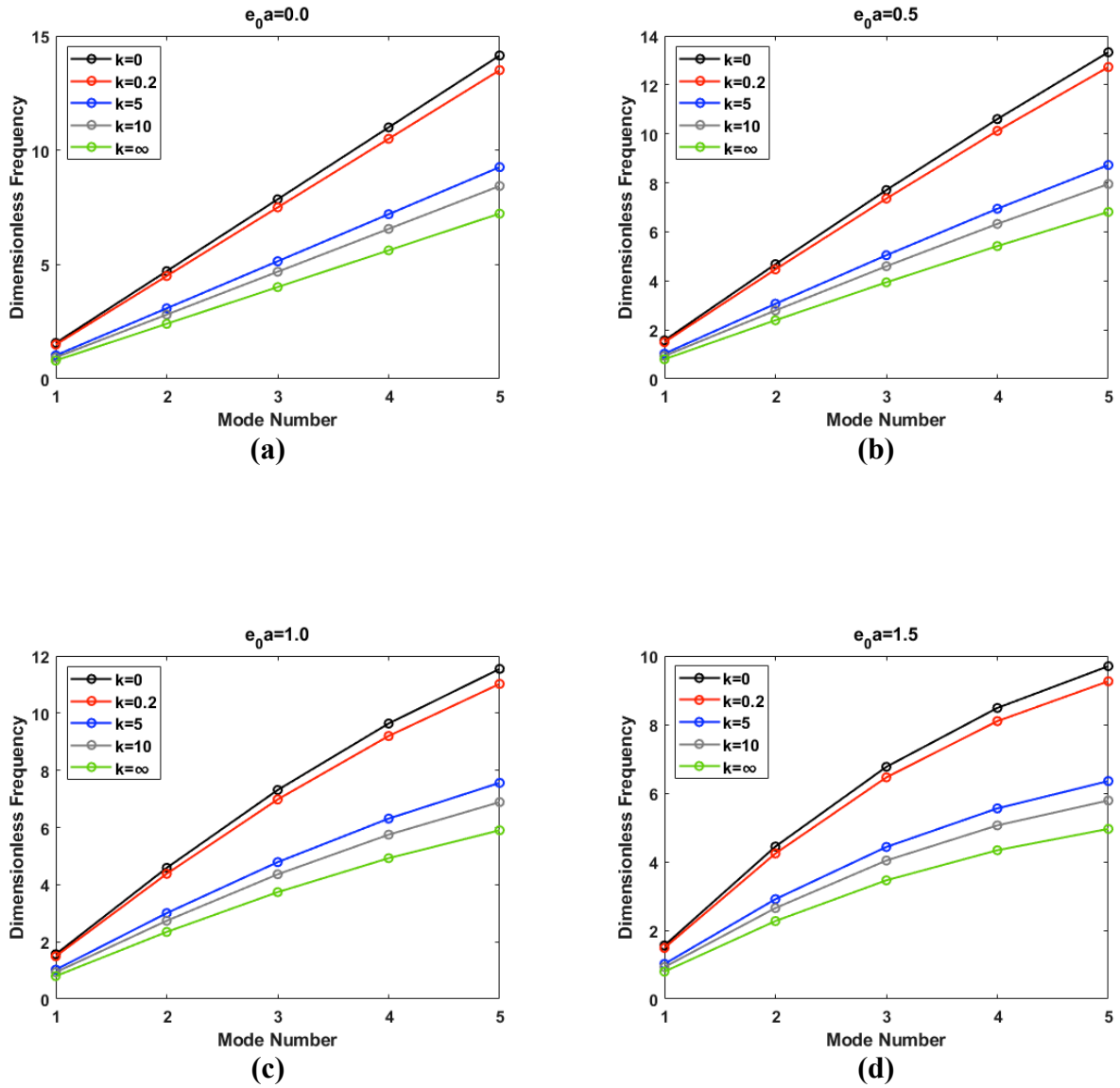

Fig. 2. Variation of dimensionless frequencies of FG nanorod

Figure 2 displays the variation of dimensionless frequencies of functionally graded nanorod with respect to mode numbers for various power-law exponent (k) and nonlocal parameter (e_0a) values. The Figure 2 is plotted from the analyses of FG nanorod with various nonlocal parameters ranging from 0 to 1.5 and various power-law exponents ranging from 0 to ∞. It is concluded from the Figure that the increasing values of power-law exponent and nonlocal parameter lead to a decrease in the dimensionless frequencies of FG nanorods. It should be noted that when the power-law exponent set to zero (k=0), the results give the frequencies of alumina (pure ceramic). If the power-law exponent sets to infinity (k=∞), the frequencies of aluminum (pure metal) are obtained. Also, if the nonlocal parameter e_0a set to zero, the frequencies of the classical theory are obtained.

5. Conclusions

In the present study, the nonlocal finite element formulation of functionally graded nanorod is proposed in conjunction with Eringen's nonlocal elasticity theory. The stiffness and mass matrices essential to the vibration response of functionally graded nanorod are found using interpolation functions. Finally, an eigenvalue problem is defined with the obtained matrices and ω_n, and the eigenvalues ω_n are found by setting the determinant of the coefficient matrix to zero. A numerical example for clamped-free boundary condition is given to investigate the influences of some parameters on frequencies of FG nanorod. The main results obtained in this study can be summarized as follows: When the nonlocal effect is ignored, that is when the e_0a value is taken as zero, the frequencies of the FG nanorod have the highest values. It is understood from that the nonlocal effect causes a reduction in the frequency of the FG nanorod. In addition, it is seen that with the increase of the power-law exponent value, that is with the transition of material properties from ceramic to metal, there is a decrease in frequencies.

References

[1] Lü, C.F., Lim, C.W. and Chen, W.Q., Size-dependent elastic behavior of FGM ultra-thin films based on generalized refined theory. *International Journal of Solids and Structures*, 46(5), 1176-1185, 2009.

[2] Lanhe, W., Thermal buckling of a simply supported moderately thick rectangular FGM plate. *Composite Structures*, 64(2), 211-218, 2004.

[3] Belkorissat, I., Houari, M.S.A., Tounsi, A., Bedia, E.A. and Mahmoud, S.R., On vibration properties of functionally graded nano-plate using a new nonlocal refined four variable model. *Steel and Composite Structures*, 18(4), 1063-1081, 2015.

[4] Żur, K.K., Arefi, M., Kim, J. and Reddy, J.N., Free vibration and buckling analyses of magneto-electro-elastic FGM nanoplates based on nonlocal modified higher-order sinusoidal shear deformation theory. *Composites Part B: Engineering*, 182, 107601, 2020.

[5] Ebrahimi, F., Ehyaei, J. and Babaei, R. Thermal buckling of FGM nanoplates subjected to linear and nonlinear varying loads on Pasternak foundation. *Advances in materials Research*, 5(4), 245, 2016.

[6] Yuan, Y., Zhao, K., Sahmani, S. and Safaei, B. Size-dependent shear buckling response of FGM skew nanoplates modeled via different homogenization schemes. *Applied Mathematics and Mechanics*, 1-18, 2020.

[7] Karami, B., Shahsavari, D., Janghorban, M. and Li, L. On the resonance of functionally graded nanoplates using bi-Helmholtz nonlocal strain gradient theory. *International Journal of Engineering Science*, 144, 103143, 2019.

[8] Uzun, B. and Yaylı, M.Ö. Nonlocal vibration analysis of Ti-6Al-4V/ZrO_2 functionally graded nanobeam on elastic matrix. *Arabian Journal of Geosciences*, 13(4), 1-10, 2020.

[9] Uzun, B., Yaylı, M.Ö. and Deliktaş, B. Free vibration of FG nanobeam using a finite-element method. *Micro & Nano Letters*, 15(1), 35-40, 2020.

[10] Uzun, B. and Yaylı, M.Ö., Finite element model of functionally graded nanobeam for free vibration analysis. *International Journal of Engineering and Applied Sciences*, 11(2), 387-400, 2019.

[11] Hosseini, S.A.H. and Rahmani, O., Free vibration of shallow and deep curved FG nanobeam via nonlocal Timoshenko curved beam model. *Applied Physics A*, 122(3), 169, 2016.
[12] Jalaei, M.H. and Civalek, Ö., On dynamic instability of magnetically embedded viscoelastic porous FG nanobeam. *International Journal of Engineering Science*, 143, 14-32, 2019.
[13] Saffari, S., Hashemian, M. and Toghraie, D., Dynamic stability of functionally graded nanobeam based on nonlocal Timoshenko theory considering surface effects. *Physica B: Condensed Matter*, 520, 97-105, 2017.
[14] Aydogdu, M., Arda, M. and Filiz, S., Vibration of axially functionally graded nano rods and beams with a variable nonlocal parameter. *Advances in nano research*, 6(3), 257, 2018.
[15] Arda, M., Axial dynamics of functionally graded Rayleigh-Bishop nanorods. *Microsystem Technologies*, 1-14, 2020.
[16] Kiani, K., Free dynamic analysis of functionally graded tapered nanorods via a newly developed nonlocal surface energy-based integro-differential model. *Composite Structures*, 139, 151-166, 2016.
[17] Arefi, M. and Zenkour, A.M., Employing the coupled stress components and surface elasticity for nonlocal solution of wave propagation of a functionally graded piezoelectric Love nanorod model. *Journal of Intelligent Material Systems and Structures*, 28(17), 2403-2413, 2017.
[18] Narendar, S., Wave dispersion in functionally graded magneto-electro-elastic nonlocal rod. *Aerospace Science and Technology*, 51, 42-51 2016.
[19] Akgöz, B. and Civalek, Ö., A size-dependent beam model for stability of axially loaded carbon nanotubes surrounded by Pasternak elastic foundation. *Composite Structures*, 176, 1028-1038, 2017.
[20] Trinh, L.C., Vo, T.P., Thai, H.T. and Nguyen, T.K. An analytical method for the vibration and buckling of functionally graded beams under mechanical and thermal loads. *Composites Part B: Engineering*, 100, 152-163, 2016.
[21] Civalek, Ö. and Kiracioglu, O. (2010). Free vibration analysis of Timoshenko beams by DSC method. *International Journal for Numerical Methods in Biomedical Engineering*, 26(12), 1890-1898, 2010.
[22] Civalek, O. and Yavas, A., Large deflection static analysis of rectangular plates on two parameter elastic foundations. *International journal of science and technology*, 1(1), 43-50, 2006.
[23] Civalek, Ö., Geometrically non-linear static and dynamic analysis of plates and shells resting on elastic foundation by the method of polynomial differential quadrature (PDQ), Ph. D. Thesis, Firat University, Elazig, 2004 (in Turkish), 2004.
[24] Civalek, Ö., Finite Element analysis of plates and shells, Elazığ: Fırat University,1998.
[25] Demir, Ç. and Civalek, Ö., A new nonlocal FEM via Hermitian cubic shape functions for thermal vibration of nano beams surrounded by an elastic matrix. *Composite Structures*, 168, 872-884, 2017.
[26] Adhikari, S., Murmu, T. and McCarthy, M.A., Dynamic finite element analysis of axially vibrating nonlocal rods. *Finite Elements in Analysis and Design*, 63, 42-50, 2013.
[27] Hemmatnezhad, M. and Ansari, R., Finite element formulation for the free vibration analysis of embedded double-walled carbon nanotubes based on nonlocal Timoshenko beam theory. *Journal of theoretical and applied physics*, 7(1), 6, 2013.
[28] Civalek, Ö., Uzun, B., Yaylı, M.Ö. and Akgöz, B. Size-dependent transverse and longitudinal vibrations of embedded carbon and silica carbide nanotubes by nonlocal finite element method. *The European Physical Journal Plus*, 135(4), 381, 2020.

[29] Ghannadpour, S.A.M., A variational formulation to find finite element bending, buckling and vibration equations of nonlocal Timoshenko beams. *Iranian Journal of Science and Technology*, *Transactions of Mechanical Engineering*, 43(1), 493-502, 2019.
[30] Akbaş, Ş.D., Static, Vibration, and Buckling Analysis of Nanobeams. *Nanomechanics*, 123, 2017.
[31] Anjomshoa, A., Shahidi, A.R., Hassani, B. and Jomehzadeh, E. Finite element buckling analysis of multi-layered graphene sheets on elastic substrate based on nonlocal elasticity theory. *Applied Mathematical Modelling*, 38(24), 5934-5955, 2014.
[32] Taghizadeh, M., Ovesy, H.R. and Ghannadpour, S.A.M. Beam buckling analysis by nonlocal integral elasticity finite element method. *International Journal of Structural Stability and Dynamics*, 16(06), 1550015, 2016.
[33] Demir, C., Mercan, K., Numanoglu, H.M. and Civalek, O., Bending response of nanobeams resting on elastic foundation. *Journal of Applied and Computational Mechanics*, 4(2), 105-114, 2018.
[34] Taghizadeh, M., Ovesy, H.R. and Ghannadpour, S.A.M., Nonlocal integral elasticity analysis of beam bending by using finite element method. *Structural Engineering and Mechanics*, 54(4), 755-769, 2015.
[35] Mahmoud, F.F., Eltaher, M.A., Alshorbagy, A.E. and Meletis, E.I., Static analysis of nanobeams including surface effects by nonlocal finite element. *Journal of mechanical science and technology*, 26(11), 3555-3563, 2012.
[36] Reddy, J.N., Energy Principles and Variational Methods in Applied Mechanics, John Wiley & Sons, 2nd Edition, 2002.
[37] Eringen, A.C., On differential equations of nonlocal elasticity and solutions of screw dislocation and surface waves. *Journal of applied physics*, 54(9), 4703-4710, 1983.
[38] Xu, X.J., Zheng, M.L. and Wang, X.C. On vibrations of nonlocal rods: Boundary conditions, exact solutions and their asymptotics. *International Journal of Engineering Science*, 119, 217-231, 2017.
[39] Numanoğlu, H.M., Akgöz, B. and Civalek, Ö. On dynamic analysis of nanorods. *International Journal of Engineering Science*, 130, 33-50, 2018.
[40] Asghari, M., Rahaeifard, M., Kahrobaiyan, M.H. and Ahmadian, M.T., The modified couple stress functionally graded Timoshenko beam formulation. *Materials & Design*, 32(3), 1435-1443, 2011.